FABRICATION OF MICRO/MESOPOROUS SILICA TUBES TEMPLATED BY ELECTROSPUN CELLULOSE ACETATE FIBERS

CHENGYING JIA,[*,**] SIYUAN HE,[**] JUNLONG SONG,[*] YONGCAN JIN,[*] WENYUAN ZHU[*] and QIANG CHENG[***]

[*]*Jiangsu Provincial Key Lab of Pulp and Paper Science and Technology, Nanjing Forestry University, Nanjing 210037, China*

[**]*Quzhou Branch of China National Pulp and Paper Research Institute, Quzhou, Zhejiang 324022, China*

[***]*Research Institute of Wood Industry, Chinese Academy of Forestry, Beijing 100091, China*

✉ *Corresponding author: Junlong Song, junlong.song@njfu.edu.cn*

Received December 14, 2015

Micro/mesoporous silica microtubes (SMTs) were fabricated with a facile approach using electrospun cellulose acetate fibers (CAEF) as template. The sol-gel reactions of tetraethoxysilane (TEOS) were employed to apply a layer of silica onto the CAEF in the media of ethanol and water, in the presence of cetyltrimethyl ammonium bromide (CTAB). The additions of CTAB, TEOS and the solvent system affected the formation of SMTs greatly. Under the optimal conditions, the SMTs were obtained after calcination with a shell thickness of about 100 nm and inner diameter from hundreds of nanometers to 1 micrometer. BET surface areas of SMTs were determined to be 765 m^2/g. The prepared SMTs are promising in drug delivery and other applications due to the combination of a hollow structure with mesopores in the walls.

Keywords: electrospinning, cellulose acetate, template, micro/mesoporous silica tubes

INTRODUCTION

Due to their combination of the advantages of hollow architecture and mesoporous nanostructure, hollow-structured mesoporous materials (HMMs) have been explored worldwide in recent years.[1-6] Their excellent performance, including low density, large specific surface area and pore volume, adjustable pore diameter, facile surface functionalization, higher guest-loading capacity than that of ordinary mesoporous materials, chemical and thermal stabilities, biodegradability, and excellent biocompatibility make HMMs an ideal candidate in applications in drug delivery, confined-space catalysis, adsorption and separation, enzyme immobilization and so on.[7-15]

In order to control the morphologic and structural parameters of materials, templates with a controllable morphology are highly advantageous.[16] Soft templates (such as emulsions, vesicles, micelles) and hard templates (such as polymers, inorganic particles, metal particles) are two most used approaches to fabricate HMMs.[17-20] The shortcoming of the soft template method is that it is difficult to prepare a metastable soft template and to control its shape, which typically results in the irregularity of HMMs.[21] Although hollow silica materials with a well-defined morphology are easily obtained with the hard template method, the removal of templates to obtain the resultant HMMs is rather complex and uneconomic.[22] Thus, developing a simple process and cost effective template with well-defined morphology remains a challenge. Wan *et al*.[23] fabricated a silica nanotube scaffold templated by bacterial cellulose (BC) with a three-dimensional network structure for potential tissue engineering application. However, the preparation of BC is complex as regards the culture and cleaning of BC pellicles.

Electrospinning is an efficient, convenient, flexible, well-known process to produce fibers with diameters ranging from tens of nanometers to a few microns.[24-27] Electrospun fibers are practical templates to fabricate tubular materials.[16,28,29] One of its advantages is that it can apply to a wide variety of substances (*e.g.* synthetic polymers,[30,31] composites,[32,33] lignocellulose,[34,35] ceramics,[36,37] oxide[38,39] *etc*.). Müller *et al*.[40] prepared both hollow silica nanofibers and silica nanotubes with independent control of core size, wall thickness, and aspect ratio templated by electrospun polyvinyl

alcohol (PVA) fibers. Silica nanotubes are employed as supports for chromium (III) half sandwich and iron (II) post metallocene catalysts and for the *in-situ* formation of polyethylene nanocomposites during ethylene polymerization.

Cellulose acetate (CA) has good filament-forming property and has abundant hydroxyl groups in its molecules, which makes its electrospun nanofibers ideal templates for tubular nanofabrication. Liu *et al*.[41] reported their work on $CaCO_3$ microtubes production using electrospun CA fibers as templates. Luo *et al*.[42] fabricated a novel carbon nanotube-containing nanofibrous polysaccharide scaffolding material *via* coating the template of electrospun CA fibers with chitosan and carbon nanotubes by the layer-by-layer (LBL) self-assembly technique.

In this study, we developed a facile method to fabricate silica micro/mesoporous tubes (SMTs) with the aid of electrospun CA fibers. The key influencing factors that would affect the morphology and the shell thickness of the silica in the formation of silica tubes were discussed in detail.

EXPERIMENTAL

Materials

Cellulose acetate (CA, 54.5-56 wt% of acetyl content) was obtained from Sinopharm Chemical Regent Co. Ltd. (Shanghai, China). All other chemicals, including acetone, tetraethoxysilane (TEOS), cetyltrimethyl ammonium bromide (CTAB), aqueous ammonia (25% w/w) and anhydrous ethanol (>99.7%) were purchased from Everbright Chemical Inc. (Nanjing, China). All chemicals were used as received without further purification. All solutions were prepared using distilled/deionized water, which was treated with a Milli-Q system (Millipore Corporation, US).

Methods

Preparation of CAEF

Electrospun CA fibers (CAEF) were produced following our earlier report[17] with some adjustments because of the different diameter demands and the different acetyl content of CA used. Briefly, a solution of CA in acetone and water (90:10 v/v) at 13 wt% concentration was loaded in a syringe equipped with a metal needle of gauge 22 (ID=1.2 mm) with a flattened tip. An aluminum foil was used as collector of electrospun fibers. The polymer solution feed rate was set at 3 mL/h. The applied voltage and the distance between the tip and the collector were of 20 kV and 15 cm, respectively.

Formation of silica@CAEF composite

The core-shell structured composite of silica@CAEF was prepared using electrospun CA fibers (CAEF) as template. CTAB was used to couple the CA fiber surfaces with the silica sol and the generators of micro- and mesopores. Water and ethanol were used as solvents, aqueous ammonia as catalyst, and TEOS as the source of silica. Initially, 20 mg of electrospun CA fibers, precisely weighed CTAB and aqueous ammonia were mixed in the solution of water and ethanol. The mixture was dispersed by ultrasonication for 30 min. Then, a precisely weighed amount of TEOS was dispersed in ethanol with 5 wt% concentration and then was slowly added into the system. After the reaction at 30 ± 1 °C for 2-3 h, the hybrid of electrospun CA fibers coated with silica (silica@CAEF) was picked up by a tweezer to move to another beaker with fresh ethanol for washing. This process was repeated twice and then the composites were dried at room temperature.

Preparation of SMTs

The final micro/mesoporous silica microtubes (SMT) were obtained by calcination of the dried silica@CAEF composite in a muffle furnace at 600 °C for 6 h to remove the organic template.

Physical and chemical characterization

Scanning electron microscopy (SEM) images of CAEF and SMT samples sputter-coated with platinum were obtained with a JEOL thermal field-emission scanning electron microscope (JSM-7600F). Transmission electron microscopy (TEM) images of SMT were obtained by a JEOL JEM-1400 and HRTEM images of SMTs were obtained by a JEOL JEM-2100 electron microscope. The powder samples for TEM measurements were dispersed in absolute ethanol with ultrasonication for 10 min and then dropped onto copper grids with carbon films.[18] Attenuated Total Reflection Fourier Transform Infrared (ATR-FTIR) spectra of CA, silica@CAEF and SMT were acquired with a Bruker VERTEX80 spectrometer. X-ray Diffraction (XRD) patterns of CA, silica@CAEF and SMT, and Small-angle XRD patterns of SMT were recorded on an Ultima IV (Rigaku Corp., Japan) with CuKα radiation. N_2 adsorption and desorption isotherms of SMT were performed using a

Micromeritics ASAP 2020 instrument. Specific surface area and pore-size distribution were determined by the Brunauer-Emmett-Teller (BET) and Barrett-Joyner-Halenda (BJH) methods.

RESULTS AND DISCUSSION

Preparation of CA electrospun fibers (CAEF)

The uniformity of the template is a key for the morphology control of silica microtubes, especially when uniform inner diameter is required. In this investigation, cellulose acetate (CA) solutions of acetone and water (9:1 v/v) with the concentrations from 10 to 17 wt% were electrospun and the CAEF were collected as a nonwoven mat in an aluminum foil. The concentration of 13% for the CA solution was found to be the optimal condition to get uniform electrospun CA fibers. As the FESEM images in Figure 1 indicate, the fibers were quite uniform, with the diameter ranging from hundreds of nanometers to 1 micrometer. One of the advantages of the electrospinning method is that it can provide uniform and continuous fibers, which will facilitate the purification process afterwards, since fibers can be picked up by tweezers and transferred to another beaker easily.

Fabrication of silica micro/mesoporous tubes (SMTs)

The surface of CAEF is relatively hydrophobic since some hydrophobic acetyl groups have replaced the hydrophilic hydroxyl groups of cellulose. The hydrophobic chain of CTAB is preferentially absorbed onto the CAEF due to hydrophobic interactions.[20,43,44] When the whole surface of CAEF is covered by CTAB, the excess CTAB will form micelles in the solution. Therefore, after CTAB addition, CAEF and CTAB micelles are positively charged. Then, TEOS is added into the system. TEOS hydrolyzes and condensates forming from the sol state to the gel one with a large quantity of hydroxyl groups, which make it negative in the solution. The negative gel is attracted by cationic CTAB and, as a consequence, the composite of silica and CAEF (silica@CAEF) is formed.

Silica micro/mesoporous tubes (SMTs) were obtained after the composites of silica@CAEF were washed and calcined. As the formation of the silica@CAEF hybrid is a vital process in the fabrication of nanotubular materials, the major parameters that influence the formation of silica tubes, including the dosages of CTAB, TEOS and solvent system, are discussed, the other conditions including dosages of catalyst-aqueous ammonia, temperature and reaction time, were set as constant at 400 μL, 30 °C and 2-3 h, respectively, throughout the investigation. After calcination, the SMT materials were characterized by TEM and FESEM.

Effect of CTAB addition on the formation of SMTs

CTAB plays multiple important roles in connecting CAEF and silica sol as a bridge, and generating micro- and mesopores. Therefore, the effect of CTAB on the formation of silica tubes needs to be firstly identified. In this part, only the CTAB charges were varied from 0 to 110 mg, while other parameters, such as the solution volume of 60 mL, TEOS dosage of 160 μL, the ratio of water and ethanol of 3:1, were maintained as constant.

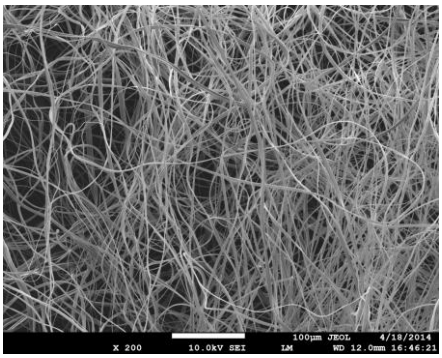

Figure 1: FESEM image of CA electrospun fibers

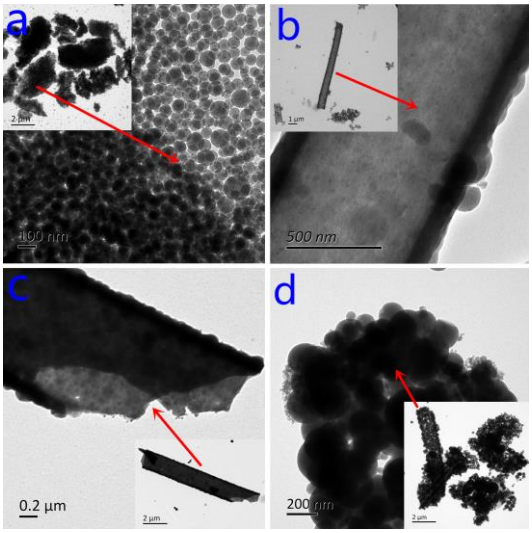

Figure 2: TEM images of silica prepared with TEOS dosage of 160 µL, in the mixture medium of 45 mL water and 15 mL ethanol, and with varied CTAB additions of (a) 11 mg, (b) 27 mg, (c) 55 mg, (d) 110 mg

As the TEM images in Figure 2 show, the shape of silica varied with the dosage of CTAB. There was nothing left after calcination when no CTAB was added (thus, there is no image in Fig. 2 for any addition of CTAB). This can be explained by the fact that no binder and any other interactions could make the silica gel absorb on the surface of CAEF, and the formed solid was washed away in the purification process. When the CTAB dosage was 11 mg, some silica sheets with the size of several micrometers were formed, but no hollow tubes can be found in the insert of Figure 2a. These silica sheets were composed of some connected silica particles with the diameter of about 50 nm, as shown in Figure 2a. When the additions of CTAB were increased further to 27 mg and 55 mg, very nice hollow and tubular structures were observed (Fig. 2b and 2c, respectively). The wall thicknesses were about 100 and 180 nm, respectively. The inner diameter of the hollow tubes was consistent with that of CAEF, ranging from hundreds of nanometers to one micrometer. While the addition of CTAB was increased to 110 mg, the tubular silica materials were composed of very large spheres with the diameter above 200 nm (Fig. 2d). The results indicate that the dosage of CTAB plays a critical role in the formation of SMTs. When the dosage is lower than 11 mg, very few CTAB micelles formed and therefore very few silica particles formed. These formed silica particles are not enough to cover the whole surface of CAEF, therefore only some silica sheets form. When the dosage is increased to 27 and then to 55 mg, these formed silica particles are enough to cover the whole surface of CAEF. As a consequence, tubular silica materials form. Meanwhile, when the dosage of CTAB is increased to a very high amount, huge CTAB micelles form, which result in huge silica particles. The proper dosage helps the materials form preferably. Therefore, 27 mg of CTAB was determined as the optimum dosage for the subsequent experiments.

Effect of solvent system on the formation of SMTs

Generally, TEOS cannot dissolve in water, so the introduction of a third solvent, which has good compatibility with both water and TEOS, would be helpful to improve the stability and homogeneity of the reaction system. We chose a non-toxic and widely used solvent – ethanol as co-solvent. The effect of the solvent system on the formation of STMs was systemically assessed in this investigation. Other parameters, such as total solution volume of 60 mL, CTAB addition of 27 mg, TEOS addition of 160 µL, were maintained as constant, while only the ratio of water to ethanol was varied from 100% to 0.

When there was a pure ethanol system, TEOS could not hydrolyze to yield silica. There was nothing left after the composite was calcined. Therefore, no image was included here. When the ratio of water and ethanol was 1:2, the diameters of the silica tubes formed were quite large and non-uniform, as presented in Figure 3a. Many scattered spheres appeared. When the ratio of water and ethanol in the solution system was 1:1, some tubular materials appeared, as can be observed in Figure

3b, however only a little amount of materials could be collected after calcination. When the ratio of water and ethanol in the solution system was 2:1, there were relatively more materials obtained after calcination and better tubular structure could be remarked (Fig. 3c). When the ratio of water and ethanol in the solution system was 3:1, the tubular materials had uniform wall structure (Fig. 3d). At last, when no ethanol was added and water was used as the only solvent in the system, only some silica fragments could be found (insert of Fig. 3e). The zoom-in image in Figure 3e illustrates that the shell was too thin and fragile. The results show that the hydrolysis of TEOS does not take place when no water exists in the system, while it slows down when there is lack of ethanol in the system. The optimal ratio of water and ethanol in the solvent system was determined to be 3:1.

Effect of TEOS addition on the formation of SMTs

TEOS is the silicon source. Its dosage has a direct effect on the wall thickness and wall uniformity of the SMTs. In this part, the influence of TEOS dosage on the wall thickness and wall uniformity of the SMTs will be discussed. Therefore, other parameters, such as solution volume of 60 mL, CTAB charge of 27 mg, the ratio of water and ethanol 3:1, were maintained as constant, and only TEOS additions were varied from 80 to 320 μL.

When TEOS dosage was 80 μL, some fractures of silica microtubes could be remarked (the insert of Fig. 4a). Based on the zoom-in image shown in Figure 4a, these fractures are composed of homogeneous silica nanoparticles. This can be explained by the fact that too little TEOS makes the wall too thin and fragile. Thus, the produced SMTs break down into fractured pieces after ultrasonication. When the additions of TEOS were increased to 160 μL and 320 μL, tubular silica materials were obtained with wall thickness of about 100 nm and 200 nm, respectively. The images are presented in Figure 4b and c, accordingly. Therefore, the wall thickness of SMTs can be fine-tuned by the TEOS dosage. Another issue related to the high dosage of TEOS is that some spherical particles were observed attached on the surface of the composite. This can be attributed to new nucleation centers formed in the case of excess TEOS. When the whole surface of CA is covered by TEOS gel and there is still excess TEOS present in the system, the silica gel may grow preponderantly around the micelle center to form global particles.

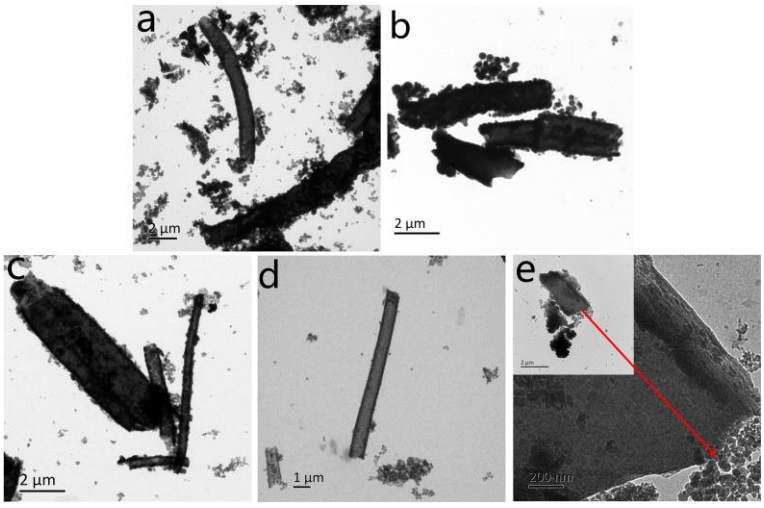

Figure 3: TEM images of silica prepared with CTAB dosage of 27 mg, TEOS dosage of 160 μL, and with varied ratios of water and ethanol (a) 20/40, (b) 30/30, (c) 40/20, (d) 45/15 and (e) 60/0 (v/v)

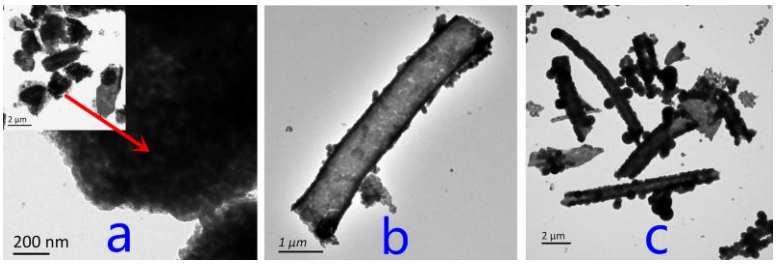

Figure 4: TEM images of silica prepared with CTAB dosage of 27 mg, aqueous ammonia dosage of 400 μL, mixture medium of 45 mL water and 15 mL ethanol, and with varied TEOS additions of (a) 80 μL, (b) 160 μL and (c) 320 μL

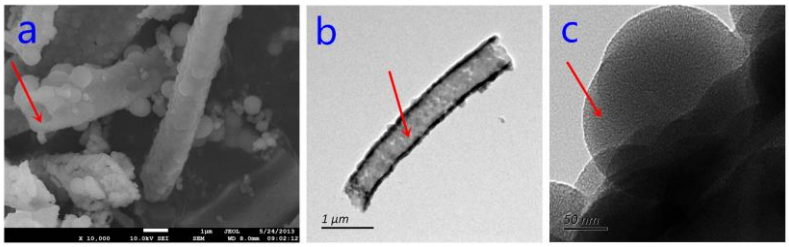

Figure 5: Field-emission electron microscopy (FE-SEM) (a) and Transmission electron microscopy (TEM) (b) images of SMTs; HRTEM image of a silica particle in the tube wall (c)

FESEM and TEM of SMTs prepared under optimum conditions

Through the experiments conducted above, the optimal conditions were determined as follows: 20 mg CAEF, 27 mg CTAB, 160 μL TEOS reacted in the mixture of 45 mL water and 15 mL ethanol. FESEM and TEM of the SMTs prepared under optimum conditions are shown in Figure 5. The tubular and hollow structure can be clearly observed in Figure 5a and Figure 5b. The wall thickness was about 100 nm. Figure 5c indicates that there are abundant distinct uniform micro- and mesopores randomly located in the silica nanoparticles composing the walls of SMTs.

Characterizations by IR, XRD and BET

The FTIR spectra of CAEF, silica@CAEF and SMTs are presented in Figure 6. The sharp peaks of CAEF and silica@CAEF at 1737 cm^{-1} and 1225 cm^{-1} exhibit the characteristic absorptions of cellulose acetate, which are attributed to the stretching vibrations of carbonyl (C=O) and (C-O), respectively. The peaks nearby 800 cm^{-1} and 450 cm^{-1} on the FTIR spectra of silica@CAEF are attributed to the symmetric stretching vibrations of Si-O-Si-. The peak at 1036 cm^{-1} in the FTIR spectrum of CAEF stands for the stretching vibrations of C-O, nevertheless, the peak at the corresponding position in the FTIR spectrum of silica@CAEF is stronger than that in the spectrum of CAEF, which is explained by the overlap of the antisymmetric stretching vibrations of Si-O-Si- and the stretching vibrations of C-O. This proves that silica has successfully coated CAEF. In the case of the FTIR spectrum of SMTs, the position of 1095 cm^{-1} corresponds to the antisymmetric stretching vibrations of Si-O-Si-, while the positions of 800 cm^{-1} and 450 cm^{-1} correspond to the antisymmetric stretching vibrations of Si-O-Si-; they are all the characteristic peaks of silica. This experiment testifies that the material fabricated is silica and the templates of CAEF and CTAB have been removed completely.

XRD results for CAEF, silica@CAEF and SMTs are presented in Figure 7. There are two wide peaks appearing at $2\theta=9°$ and 18° for CAEF, which hints that electrospun CA fibers are composed mostly of amorphous regions. The 2θ of silica@CAEF appears as a stronger full peak at 18°, compared with that of CAEF. This can be attributed to the silica layer coated on CAEF. The 2θ of SMTs turns up as a stronger full peak at about 20°, which is the characteristic peak of silica materials. This result proves that the material fabricated is silica and its crystallinity is quite low.

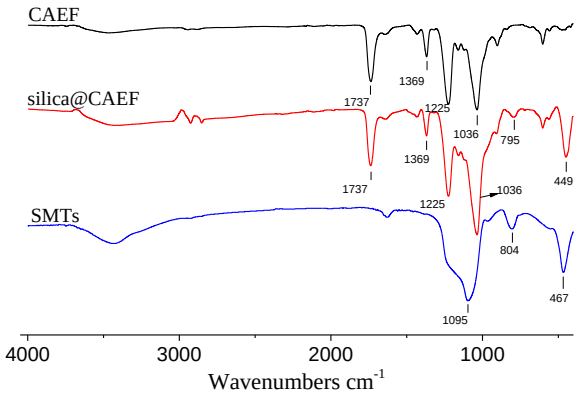

Figure 6: FTIR spectra of CAEF, silica@CAEF and SMTs

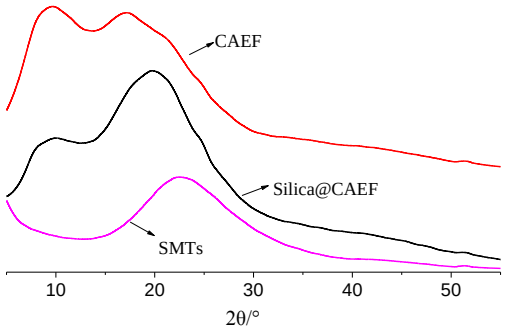

Figure 7: XRD patterns of CAMF, silica@CAEF and SMTs

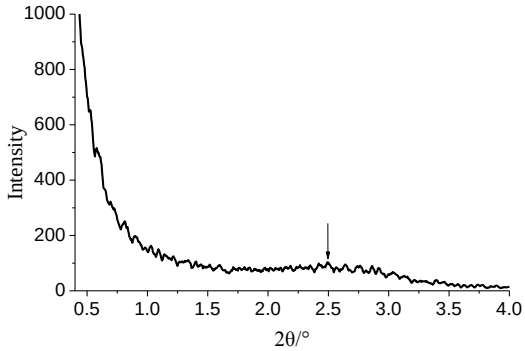

Figure 8: Small-angle X-ray diffraction (XRD) pattern of micro/mesoporous silica tubes

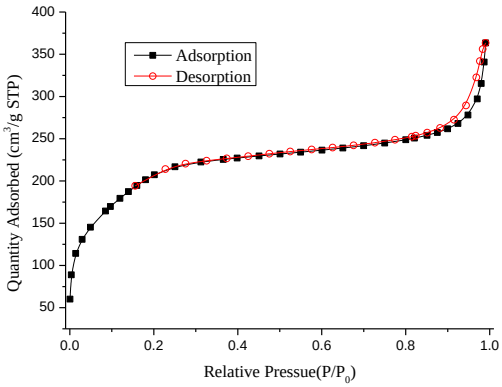

Figure 9: Nitrogen adsorption-desorption isotherms of micro/mesoporous silica tubes

The small-angle XRD pattern in Figure 8 presents a weak peak located at about 2θ=2.5°. The materials with such XRD patterns are usually regarded as 'X-ray amorphous' materials, which are usually divided into four broad categories: disordered nanocrystalline, glassy, amorphous, and mixed systems.[45] The pattern indicates that the micro- and mesopores in the tube wall are disordered.

The nitrogen adsorption-desorption isotherm measurement was employed to characterize the surface areas and pore volume of the obtained SMTs. As shown in Figure 9, N_2 adsorption significantly increases with the partial pressure increasing under the lower relative pressure (P/P_0 < 0.2), caused by micropores and mesopores. The sample exhibits the capillary condensation process at P/P_0 from 0.3 to 1. The loop observed at the relative pressure (P/P_0) ranging from 0.45 to 0.85 indicates that mesopores exist. The sharp capillary condensation step occurring at relative pressures (P/P_0) between 0.45 and 0.85 is evidence of the existence of macropores in the materials. The adsorption-desorption isothermal plot can be assigned to a combination of type IV and type I according to IUPAC 13.2. It belongs to a micro/mesoporous material.

By analyzing the adsorption isotherm, it can be concluded that the samples possess a high BET (Brunauer Emmett Teller) surface area of about 765.4 m^2/g, a pore size of 4.6 nm, and a total pore volume of 0.41 cm^3/g (calculated by the BJH method). The microporous median pore width is of about 0.7 nm, and its maximum pore volume is of about 0.18 cm^3/g (calculated by the Horvath-Kawazoe pore size distribution analysis). The porous and hollow structure of SMTs makes the material promising in drug delivery and other applications.[15]

CONCLUSION

In conclusion, micro/mesoporous silica microtubes were fabricated with a simple method using CA electrospun fibers as template, CTAB as pore generator and bridging connector between CAEF and silica nanoparticles, a proper mixture of water and ethanol as solvent, aqueous ammonia as catalyst, and TEOS as silica source and as a key parameter to control the wall thickness of SMTs. The dosage of CTAB, TEOS and the ratio of ethanol-to-water affected the morphology of SMTs greatly. The prepared mesoporous silica nanotubes were quite uniform with inner diameters in the range from hundreds of nanometers to 1 micrometer, and thicknesses of the shell of about 100 nm. The nitrogen adsorption-desorption explained that the materials were micro and mesoporous. BET specific surface area for the tubular silica was as high as 765.4 m^2/g. This SMT material is promising in drug delivery and other applications due to its combined characteristics of hollow structure and mesopores in the walls.

ACKNOWLEDGEMENTS: The authors are grateful for the support of the Special Fund for Forestry Scientific Research in the Public Interest (201404510), National Natural Science Foundation of China (31270613, 31200454), Qing-lan Project, the Priority Academic Program Development of Jiangsu Higher Education Institutions, and Jiangsu Co-Innovation Center for Efficient Processing and Utilization of Forest Resources (Nanjing Forestry University).

REFERENCES

1 M. Priebe and K. M. Fromm, *Chemistry*, **21**, 3854 (2015).
2 A. H. Lu and F. Schüth, *Adv. Mater.*, **18**, 1793 (2006).
3 Y. Li and J. Shi, *Adv. Mater.*, **26**, 3176 (2014).
4 S. H. Wu, C. Y. Mou and H. P. Lin, *Chem. Soc. Rev.*, **42**, 3862 (2013).
5 A. Popat, S. B. Hartono, F. Stahr, J. Liu, S. Z. Qiao *et al.*, *Nanoscale*, **3**, 2801 (2011).
6 D. T. Mitchell, S. B. Lee, L. C. M. Trofin, N. Li, T. K. Nevanen *et al.*, *J. Am. Chem. Soc.*, **124**, 11864 (2002).
7 J. H. Jung, M. Park and S. Shinkai, *Chem. Soc. Rev.*, **39**, 4286 (2010).
8 W. Huang, Y. Zhu, J. Tang, X. Yu, X. Wang *et al.*, *J. Mater. Chem. A*, **2**, 8839 (2014).
9 H. Zhang, R. Jin, H. Yao, S. Tang, J. Zhuang *et al.*, *Chem. Commun.*, **48**, 7874 (2012).
10 F. Tang, L. Li and D. Chen, *Adv. Mater.*, **24**, 1504 (2012).
11 D. Wang, Z. Xu, Z. Chen, X. Liu, C. Hou *et al.*, *ACS Appl. Mater. Interfaces*, **6**, 12600 (2014).
12 J. Shen, G. Song, M. An, X. Li, N. Wu *et al.*, *Biomaterials*, **35**, 316 (2014).
13 Q.-G. Xiao, X. Tao, H.-K. Zou and J.-F. Chen, *Chem. Eng. J.*, **137**, 38 (2008).
14 S. Cao, L. Fang, Z. Zhao, Y. Ge, S. Piletsky *et al.*, *Adv. Func. Mater.*, **23**, 2162 (2013).
15 C. Jia, J. Song, Y. Jin and O. J. Rojas, *J. Appl. Polym. Sci.*, **132**, DOI: 10.1002/app.42562 (2015).
16 S. Nagamine, Y. Tanaka and M. Ohshima, *Chem. Lett.*, **38**, 258 (2009).
17 J. Song, N. L. Birbach and J. P. Hinestroza, *Cellulose*, **19**, 411 (2012).
18 J. L. Song, G. S. Fu, Q. Cheng and Y. C. Jin, *Ind. Eng. Chem. Res.*, **53**, 708 (2014).
19 J. L. Song, C. X. Wang and J. P. Hinestroza, *Cellulose*, **20**, 1727 (2013).
20 J. L. Song and O. J. Rojas, *Nord. Pulp Pap. Res. J.*, **28**, 216 (2013).
21 Z. Chen, D. Niu, Y. Li and J. Shi, *RSC Adv.*, **3**, 6767 (2013).
22 Z. Feng, Y. Li, D. Niu, L. Li, W. Zhao *et al.*, *Chem. Commun.*, 2629 (2008).
23 Y. Wan, P. Liu, C. Zhang, Z. Yang, G. Xiong *et al.*, *J. Alloy. Compd.*, **647**, 711 (2015).
24 S. Rafiei, S. Maghsoodloo, M. Saberi, S. Lotfi, V. Motaghitalab *et al.*, *Cellulose Chem. Technol.*, **48**, 401 (2014).
25 N. Bhardwaj and S. C. Kundu, *Biotechnol. Adv.*, **28**, 325 (2010).
26 C. L. Zhang and S. H. Yu, *Chem. Soc. Rev.*, **43**, 4423 (2014).
27 X. Lu, C. Wang and Y. Wei, *Small*, **5**, 2349 (2009).
28 Y. Qiu and J. Yu, *Solid State Commun.*, **148**, 556 (2008).

[29] S. Li, X. Yue, Y. Jing, S. Bai and Z. Dai, *Colloid*. *Surface*. *A*, **380**, 229 (2011).
[30] T. Subbiah, G. S. Bhat, R. W. Tock, S. Parameswaran and S. S. Ramkumar, *J*. *Appl*. *Polym*. *Sci*., **96**, 557 (2005).
[31] Z.-M. Huang, Y. Z. Zhang, M. Kotaki and S. Ramakrishna, *Compos*. *Sci*. *Technol*., **63**, 2223 (2003).
[32] H. Kang, Y. Zhu, X. Yang, Y. Jing, A. Lengalova *et al*., *J*. *Colloid Interf*. *Sci*., **341**, 303 (2010).
[33] C. Tsioptsias, K. G. Sakellariou, I. Tsivintzelis, L. Papadopoulou and C. Panayiotou, *Carbohyd*. *Polym*., **81**, 925 (2010).
[34] Y. Ahn, S. H. Lee, H. J. Kim, Y.-H. Yang, J. H. Hong *et al*., *Carbohyd*. *Polym*., **88**, 395 (2012).
[35] Y. Ahn, D. H. Hu, J. H. Hong, S. H. Lee, H. J. Kim *et al*., *Carbohyd*. *Polym*., **89**, 340 (2012).
[36] P. K. Panda, *T*. *Indian Ceram*. *Soc*., **66**, 65 (2014).
[37] A. Guo, J. Liu, Y. Wang and H. Xu, *Mater*. *Lett*., **74**, 107 (2012).
[38] L.-D. Kim, A. Rothschild, B. H. Lee, D. Y. Kim, S. M. Jo *et al*., *Nano Lett*., **6**, 2009 (2006).
[39] D. Lin, H. Wu, R. Zhang and W. Pan, *Chem*. *Mater*., **21**, 3479 (2009).
[40] G. F. J. Müller, M. Stürzel and R. Mülhaupt, *Polymer*, **55**, 465 (2014).
[41] L. Liu, D. He, G. S. Wang and S. H. Yu, *Langmuir*, **27**, 7199 (2011).
[42] Y. Luo, S. Wang, M. Shen, R. Qi, Y. Fang *et al*., *Carbohyd*. *Polym*., **91**, 419 (2013).
[43] J. Song, Y. Li and Q. Cheng, *J*. *Appl*. *Polym*. *Sci*., **131**, 9903 (2014).
[44] J. L. Song, W. E. Krause and O. J. Rojas, *J*. *Colloid Interface Sci*., **420**, 174 (2014).
[45] Y. Zhang, X. Liu and J. Huang, *ACS Appl*. *Mater*. *Interfaces*, **3**, 3272 (2011).